CO_3^{2-} — HCO_3^- 溶液中 X80 管线钢焊接接头的应力腐蚀开裂分析

王炳英， 霍立兴， 张玉凤， 王东坡
（天津大学 材料科学与工程学院，天津 300072）

王炳英

摘 要：采用慢应变速率试验（SSRT）、扫描电镜（SEM）观察研究了国产 X80 管线钢焊接接头在 0.5 mol/L Na_2CO_3 + 1 mol/L $NaHCO_3$ 溶液中的应力腐蚀开裂（SCC）敏感性。结果表明，拉伸试样全部断裂在焊缝或热影响区。在所研究的电位区间，拉伸试样随着外加电位正向增加，断面收缩率、断裂时间和断后伸长率增加，而断口部位的裂纹平均扩展速率减小，SCC 敏感性降低。试样断口形貌在阴极电位条件下呈准解理断裂，在自腐蚀电位和阳极电位条件下，焊缝试样断口主要是韧性断裂。应力腐蚀机理可以用阳极溶解理论和氢致破裂来解释。

关键词：X80 管线钢；焊接接头；慢应变速率试验；应力腐蚀开裂
中图分类号：TG172.9 文献标识码：A 文章编号：0253－360X（2007）07－085－04

0 序 言

自从 20 世纪 60 年代中期 Wenk 首次发现埋地管线的高 pH 值应力腐蚀（SCC）环境以来，出现了许多与 SCC 有关的管线失效事例[1,2]。其相应的研究报道主要局限低于 X70 强度级别的管线钢[3－5]。国产 X80 管线钢在高 pH 值模拟土壤介质中应力腐蚀的研究尚未有报道。

X80 管线钢是采用微合金控轧技术研制，强度高，韧性好，是目前国内使用的最高强度级别的管线钢，已少量铺设在“西气东输”工程中。管道铺设距离长，所经地形地貌复杂，土壤介质成分复杂，由于焊接接头存在较大的残余应力和组织性能的不均匀性，所以加强对国产 X80 管线钢焊接接头应力腐蚀的研究有着重要的工程应用价值，实验室多采用 0.5 mol/L Na_2CO_3 + 1 mol/L $NaHCO_3$ 溶液模拟管道材料高 pH 值 SCC 的研究[6]。

作者对国产 X80 管线钢及焊接接头试样在高 pH 值模拟土壤介质中的 SCC 进行实验室研究。采用慢应变速率拉伸（SSRT）、扫描电镜（SEM）和金相组织观察研究其在不同电位下的 SCC 敏感性，并用显微组织变化和电化学理论分析 SCC 发生的机理。

1 试验材料及方法

1.1 X80 钢的化学成分和力学性能

试验所用材料为国产的 X80 管线钢，其化学成分如表 1 所示，力学性能如表 2 所示。焊接接头取自埋弧焊直缝焊管。

表 1 X80 母材的化学成分（质量分数，%）

Table 1 Chemical composition of X80 pipeline steel

C	Mn	Si	P	S	Mo	Ni	Cr	Nb	Ti	Al	N	B	V+Nb+Ti
0.050	1.780	0.220	0.007	0.003	0.260	0.256	0.027	0.055	0.015	0.044	0.007	0.000 1	0.072

1.2 试验方法及过程

试样取自环焊缝纵向。按照慢应变拉伸试验机的要求制作，其形状和尺寸如图 1 所示，其中焊缝位于焊接接头试样标距中间。试样拉伸前，标距区经过 150 号～700 号金相砂纸打磨后，用无水乙醇清洗，丙酮脱脂。

试验溶液，采用 0.5 mol/L Na_2CO_3 + 1 mol/L $NaHCO_3$ 溶液。

收稿日期：2006－08－23

表 2 X80 管线钢及焊缝的力学性能

Table 2 Mechanics properties of X80 pipeline steel and weld

名称	规定总延伸强度 $R_{r0.5}$/MPa	抗拉强度 R_m/MPa	断后伸长率 A(%)	屈强比 $R_{r0.5}/R_m$
X80 管线钢	596	693	38	0.86
焊缝	608	729	37	0.83

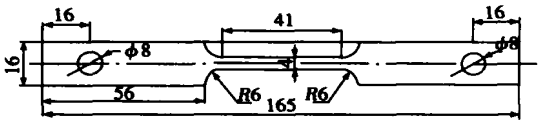

图 1 X80 钢焊接接头 SSRT 试样(mm)

Fig. 1 Sketch of SSRT specimen of X80 steel welded joint

试验温度为室温。

试验程序, 试验开始前, 分别将试样两端安装在试验装置上, 其它部分全部浸泡在试验溶液中。试样在拉伸过程中由 M273 恒电位仪施加外加电位, 采用三电极体系, 辅助电极为铂片, 参比电极为饱和甘汞电极(SCE), 文中电位值均相对于 SCE。试验过程中由计算机自动控制, 并记录载荷 — 时间曲线。试样拉断后, 对断口进行 SEM 观察。

1.3 试验评定参数

根据国家标准 GB/T15970.7 — 2000《慢应变速率试验》, 可用断裂时间 t_f, 断后伸长率 A, 断面收缩率 Z 等参数来判定不同电位条件下焊缝拉伸试样 SCC 的敏感性。

2 试验结果及讨论

2.1 SSRT 试验的拉伸曲线

采用国产 SCC — 1 型慢应变拉伸试验机进行应力腐蚀试验, 应变速率为 $1.0\times10^{-6}\ s^{-1}$。分别测试了 0.5 mol/L Na_2CO_3 + 1 mol/L $NaHCO_3$ 溶液中拉伸试样在不同外加电位下的应力 — 拉伸曲线。从图 2 中可以看出, 应力 — 应变曲线的变化具有一定的规律性。空拉时无论是抗拉强度还是断裂寿命都是最大的; 当有外加电位时, 随着电位的负向增大, 断裂寿命却逐渐降低, 呈现下降趋势。

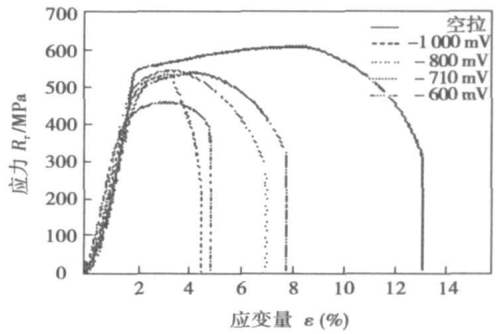

图 2 不同外加电位下 X80 钢焊接接头的应力 — 应变曲线

Fig. 2 Stress-strain curve of X80 pipeline steel welded joints in different applied potential

2.2 外加电位对 SCC 敏感性的影响

拉伸试样在不同外加电位下的 SSRT 结果如表 3 所示。表 3 表明, 随电位的正向增加, 焊接接头试样的断面收缩率 Z, 断裂寿命 t_f 和应变量 ε 均明显增加, CGR(裂纹扩展速率, 即最大裂纹深度与断裂时间的比值)明显降低, 试样 SCC 敏感性降低。相对自腐蚀电位而言, 施加阴极电位时, 断裂寿命 t_f 明显降低, CGR 明显增大; 而外加阳极电位, 断裂时间 t_f 变化不大, 但 CGR 变小很多。焊接接头的断裂位置多发生在 HAZ 处, 可见 HAZ 是焊接接头试样的 SCC 敏感区。

2.3 断口分析

图 3 是不同外加电位下 SSRT 断裂试样的断口形貌。在 −1 000 mV 时, 试样断裂面与拉伸轴方向垂直, 断口呈泥状花样, 明显的准解理断裂。阴极电位为 −800 mV 时, 断口为准解理断裂 + 韧性断裂混合型, 如图 3d, e 所示。

表 3 X80 管线钢焊接接头的应力腐蚀断裂参数

Table 3 Stress corrosion cracking parameters of X80 pipeline steel welded joints

试样取材部位	外加电位 φ/mV	断裂寿命 t_f/h	断面收缩率 Z(%)	应变量 ε(%)	裂纹扩展速率 CGR/(μm·h^{-1})	断裂位置
焊接接头	−1 000	12.96	29.84	1.86	11.69	HAZ
	−800	13.40	35.60	2.00	11.23	HAZ
	−710	19.29	42.50	2.87	1.56	HAZ
	−600	21.44	61.92	3.19	0.61	HAZ
	空拉	35.96	74.00	4.67	—	焊缝

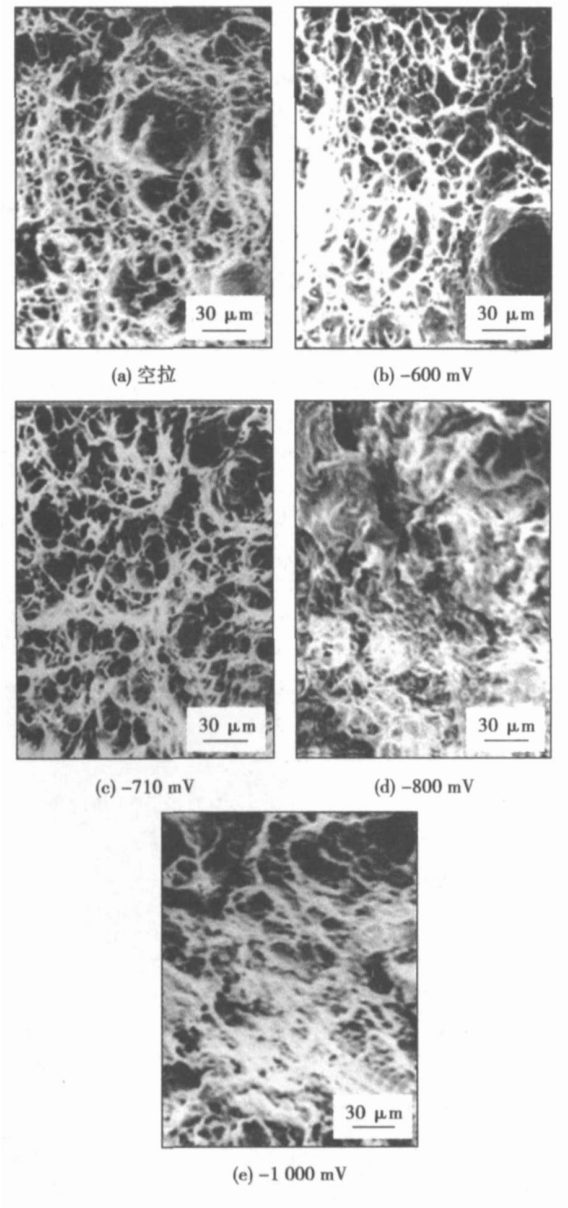

图 3　不同外加电位下 X80 管线钢焊接接头拉伸试样的断口形貌

Fig. 3　Fracture pattern of tension specimen of X80 pipeline steel welded joints in different applied potential

在空拉状态、阳极电位－600 mV 以及自腐蚀电位－710 mV 时，X80 管线钢焊接接头 SSRT 试验结果表明，试样发生断裂时，可以发现试样断裂面为斜断口，与拉伸轴方向大致成 45° 角，扫描电镜对断口进行观察，如图 3a，b，c 所示，其断口形貌主要是韧窝形的韧性断裂。

2.4　应力腐蚀试验分析

试验结果（图 2 和表 3）表明，X80 管线钢焊接接头在 0.5 mol/L Na_2CO_3＋1 mol/L $NaHCO_3$ 溶液中的敏感部位是HAZ。热影响区由于受到焊接热循环作用致使组织和性能发生变化，HAZ 发生局部的硬化、脆化和韧性降低，并且 HAZ 仍然受到焊接残余拉应力的作用，两方面的原因致使拉伸试样的 HAZ 成为SCC 的敏感区域。

在 0.5 mol/L Na_2CO_3＋1 mol/L $NaHCO_3$ 溶液中 X80 钢可能发生下列反应[7]。

阳极反应　$Fe \rightarrow Fe^{2+} + 2e$，　（1）

$$Fe^{2+} + HCO_3^- \rightarrow FeCO_3 + H^+ + 2e，\quad (2)$$

$$FeCO_3 + 3H_2O \rightarrow \gamma - Fe_2O_3 + 2HCO_3^- + 2e。\quad (3)$$

阴极反应　$H^+ + e \rightarrow H$。　（4）

金属铁在电流作用下不断溶解生成 Fe^{2+}，溶解的 Fe^{2+} 与 HCO_3^- 反应生成 $FeCO_3$，$FeCO_3$ 进一步反应生成稳定的 $\gamma-Fe_2O_3$，覆盖在金属表面，形成致密而稳定的钝化膜。在慢应变拉伸条件下，应力使金属塑性变形，位错发生运动，在表面产生滑移台阶，使 $\gamma-Fe_2O_3$ 钝化膜破裂，裸露金属与介质接触发生快速溶解，裂纹以溶解方式向前扩展，形成微裂纹[8]，在该溶液中 X80 管线钢焊接接头的极化曲线（图 4）测试可以验证这一过程的产生。

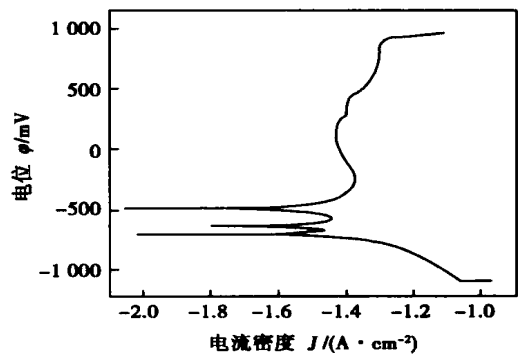

图 4　X80 管线钢焊接接头的极化曲线

Fig. 4　Polarization curves of X80 pipeline steel welded joint

当施加阴极电位时，$\varphi < \varphi_{corr}$，反应式（4）的反应速度增加，溶液中氢浓度增加。微裂纹中生成氢在裂尖局部浓缩，导致裂尖脆化，在应力作用下裂纹发生扩展。试验结果（表 3）表明随外加电位的负向增大，SCC 敏感性增加，可以验证 SCC 与氢浓度有直接的关系。焊缝金属、母材显微组织以针状铁素体为主，HAZ 以粒状贝氏体为主，其晶内都存在很高的位错密度[9]。而氢对位错有钉扎作用，使位错运动受阻，形成位错塞积，发生应力集中导致微裂纹的扩展。在自腐蚀电位和阳极电位条件下，不利于反应式（4）的进行，溶液中氢浓度很低，氢的作用很小，断口 SCC 敏感性降低，其断口形貌呈现明显的韧性断裂，这一阶段，氢的影响很小[10]。

X80 管线钢焊接接头的应力腐蚀可以用阳极溶

解理论和析氢腐蚀理论来解释。

3 结 论

(1) 在 0.5 mol/L Na_2CO_3 + 1 mol/L $NaHCO_3$ 溶液中, 随着外加电位的正向增大, X80 管线钢焊接接头试样的断裂寿命、断面收缩率和应变量明显增加, 断口 SCC 的裂纹平均扩展速率降低, SCC 敏感性降低。

(2) 焊接接头试样在不同外加电位下进行慢应变速率试验后, 断口形貌在阴极电位条件下呈准解理断裂, 在自腐蚀电位和阳极电位条件下, 焊接接头试样断口主要以韧性断裂为主。

(3) X80 管线钢的应力腐蚀是阳极溶解和析氢腐蚀共同作用的结果。

参考文献:

[1] Rebak R B, Xia Z, Safruddin R, *et al*. Effect of solution composition and electrochemicol potential on stress corrosion cracking of X-52 pipeline steel[J]. Corrosion, 1996, 52(5): 396-405.

[2] Parkins R N, Bellhimer E, Blanchard W K. Stress corrosion cracking characteristics of a ranger of pipeline steels in carbonate-bicarbonate solution[J]. Corrosion, 1993, 49(12): 951-966.

[3] Parkins R N. Mechanistic aspects of intergranular stress corrosion cracking of ferritic steels[J]. Corrosion, 1996, 52(5): 363-374.

[4] 闫茂成, 翁永基. 环境溶液对管道应力腐蚀过程电化学行为的影响[J]. 中国腐蚀与防护学报, 2005, 25(1): 34-38.

[5] 李明星, 王 荣, 李鹏亮, 等. X70 管线钢在模拟土壤介质中裂纹扩展量化模型[J]. 中国腐蚀与防护学报, 2004, 24(3): 163-167.

[6] Delanty B, O'Beime J. Major field study compares pipeline SCC with coatings[J]. Oil Gas Journal, 1992, 90(24): 39-44.

[7] Blengino J M, Keddam M, Labbe J P, *et al*. Physico-chemical characterization of corrosion layers formed on iron in soditum carbonate-bicarbonate containing environment[J]. Corosion Science, 1995, 37: 621-643.

[8] 方丙炎, 王俭秋, 朱自勇, 等. 埋地管线在近中性 pH 和高 pH 环境中的应力腐蚀开裂[J]. 金属学报, 2001, 37(5): 453-458.

[9] 王炳英, 霍立兴, 张玉凤, 等. X80 管线钢焊接接头的硫化氢应力腐蚀试验研究[J]. 压力容器, 2006, 23(7): 15-18.

[10] 黄春波, 李光福, 杨 武. X70 管线钢焊缝应力腐蚀破裂的研究[J]. 腐蚀与防护, 2005, 26(1): 1-5.

作者简介: 王炳英, 女, 1972 年出生, 副教授, 博士研究生。主要研究方向为材料强度与断裂研究。发表论文 10 篇。

Email: tdwby2004@126.com

[上接第 84 页]

of Materials Processing Technology, 2003, 134: 174-179.

[4] Erich Folkhard. 不锈钢焊接冶金[M]. 栗卓新, 朱学军, 译. 北京: 化学工业出版社, 2004.

[5] Pickerring F B. Some beneficial effects of nitrogen in steel[C] // Conference HNS-88, Lille, France, May 18-20, 1988. The Institute of Metals, London, 1989.

[6] Schino A D, Kenny J M. Grain refinement strengthening of a microcrystalline high nitrogen austenitic stainless steel[J]. Materials Letters, 2003, 57: 1830-1834.

[7] Mudali U K, Baldev R. 高氮钢和不锈钢——生产、性能与应用[M]. 李 晶, 黄运华, 译. 北京: 化学工业出版社, 2006.

作者简介: 张田宏, 女, 1975 年出生, 硕士, 高级工程师。主要从事船体结构钢及配套焊接材料的开发及应用研究工作。发表论文 10 余篇。

Email: vila_zhang@tom.com

relationship between the energy density and the welding time was approximately linear. And the welding time as well as the axial shortening increased with the energy density. Furthermore increasing the energy density produced an increase in the temperature of the interface and also an increase in the flash generated during the welding process. The calculated data of the welding time and axial shortening during welding were in good agreement with the measured data.

Key words: inertia friction welding; GH4169 alloy; energy density; numerical simulation

Pulsed MIG welding equipment based on DSP control

YANG Wenjie, LIAO Ping (School of Materials Science and Engineering, Jiamusi University, Jiamusi 154007, Heilongjiang, China). p77—80

Abstract: The structure of pulsed MIG (metal inert-gas) welding equipment, which adopts inverter technology using IGBT, is designed based on DSP chip TMS320F2812 and mainly uced on aluminum alloys. Welding control system comprises hardware and software, using C language welding program, and it reduces difficulty of control system exploitation. Scheduling control, sampling disposal of feedback signals and digital PI modulation are achieved through program control, and this controls veraciously welding process. Experimental results validated that this welding equipment is character with high control precision and stability, it can obtain better appearance of weld.

Key words: pulsed metal inert-gas; digital signal processing; inverter

Effect of carbon and nitrogen on microstructure and properties of austenite weld metal

ZHANG Tianhong, DU Yi, ZHANG Junxu (Luoyang Ship Material Research Institute, Luoyang 471039, Henan, China). p81—84, 88

Abstract: Effect of carbon and nitrogen on microstructure and properties of austenite weld metal were studied by scanning electron microscope, transmission electron microscope and other methods. With increasing C content, the quantity of $M_{23}C_6$ carbide particles at austenite grain boundaries increased and the size of $M_{23}C_6$ enlarged. The tensile strength of deposited metal increased, however, the toughness decreased markly. When the content of C increases to a high level, the solution strengthening effect doesn't express anymore, but the quantity and size of carbide particles formed at austenite grain boundartes is still increasing. The toughness and intergranular corrosion resistance decreased continuously. With increasing N content, tensile strength increased, at the same time, the toughness kept at high level. Owing to small quantity of carbide particles formed at austenite grain boundaries, intergranular corrosion resistance displayed good performance.

Key words: austenitic electrode; tensile strength; toughness; carbide

CO_3^{2-} — HCO_3^- stress corrosion test of welded joint for X80 pipeline steel

WANG Bingying, HUO Lixing, ZHANG Yufeng, WANG Dongpo (School of Material Science and Engineering, Tianjin University, Tianjin 300072, China). p85—88

Abstract: The susceptibility to stress corrosion cracking (SCC) of the welded joint of X80 pipeline steel in solution of 0.5 mol/L Na_2CO_3 and 1mol/L $NaHCO_3$ was investigated by means of slow strain rate testing (SSRT) and scanning electron microscope. The results showed that all tensile test specimens cracked in welded joint and heat affected zone (HAZ). The general tendency in the studied potential range was that with positive increasing of potential, reduction in area, fracture time and elongation of specimens increased, and mean crack growth rate of SCC and the susceptibility to SCC decreased. At cathodic potentials, obvious quasi-cleavage fracture was observed in the fracture area of specimens. At open circuit potential and anodic potential, ductile fracture was the common fracture pattern. The mechanism of the stress corrosion could be explained with anodic solution theory and hydrogen induced cracking.

Key words: X80 pipeline steel; welded joint; slow strain rate testing; stress corrosion crack

Numerical simulation of welding temperature distribution for Ni-base superalloy little section square-tube

WANG Junheng, ZHANG Guangjun, GAO Hongming, WU Lin (State Key Laboratory of Advanced Welding Production Technology, Harbin Institute of Technology, Harbin 150001, China). p89—93

Abstract: The welding temperature field of Ni-based superalloy little-section rectangular tube is calculated by using non-contact model. After comparing the simulating results with the measuring ones it indicates big errors when applying this model to the temperature field of little section rectangular in welding simulation. By analyzing the relationship between little-section rectangular tube and welding positioner in the view of mechanic and thermal perspectives, the reason for the errors of simulating results is found out. Based on this reason, the contact model is presented. The heat transfer and stress analysis between little-section rectangular tube and welding positioner are simulated by using direct constraints method, and then the laws of the temperature distribution are gotten. The experimental results show that a "T" shaped temperature-field distribution is formed in the vicinity of the weld. After cooling for a period of time, the temperature distribution of the weldments shows that a lower temperature region exists at both ends, and a higher temperature region exists in the middle of the tube. The computed results are in good agreement with the experimentally measured results.

Key words: little-section rectangular tube; contact; direct constraints method; temperature field

Microstructures and crack resistance of armoured steel weldment by CO_2 shielded arc welding

ZHU Xiaoying, TAN Wei, ZHAO Yang (National Key Laboratory for Remanufacturing, Academy of Armord Forces Engineering, Beijing 100072, China). p94—96

Abstract: The armoured steel welded joints were prepared by CO_2 shielded arc welding with modified H10MnSi wire and H08Mn2Si wire respectively. The microstructures of the welded